THE ASTROPHYSICAL JOURNAL, 477:926–939, 1997 March 10

DERIVING THE GEOMETRY OF Be STAR CIRCUMSTELLAR ENVELOPES FROM CONTINUUM SPECTROPOLARIMETRY. I. THE CASE OF ζ TAURI

KENNETH WOOD, K. S. BJORKMAN,[1] AND J. E. BJORKMAN[1]
Department of Astronomy, University of Wisconsin, 475 North Charter Street, Madison, WI 53706;
kenny@madraf.astro.wisc.edu
Received 1996 July 26; accepted 1996 September 23

ABSTRACT

We present a general scheme for determining the circumstellar geometry of Be stars from modeling of optical continuum spectropolarimetry. Our modeling scheme utilizes a Monte Carlo radiation transfer code that determines the polarization due to multiple photon scattering, including the effects of continuous hydrogen absorption and emission from a disklike circumstellar envelope. We show that by matching the polarization level on either side of the Balmer jump, one can determine the opening angle of the disk. In general, there are only two solutions, either a geometrically thin or a geometrically thick disk.

Applying our analysis techniques to observations of the Be star ζ Tauri, we find that the two solutions for the disk have half-opening angles of either 2°.5 or 52°. The geometricaly thick disk can be excluded based on recent interferometric imaging of Be star disks, including ζ Tau. The thin disk solution is consistent with *either* a Keplerian or a wind-compressed disk; both models predict small disk opening angles at small radii. In addition to matching the continuum polarization, our thin disk model reproduces the continuum spectral energy distribution from the UV through *IRAS* wavelengths, providing convincing evidence that Be circumstellar disks are geometrically thin.

Subject headings: circumstellar matter — polarization — radiative transfer — stars: emission-line, Be — stars: individual (ζ Tauri)

1. INTRODUCTION

Be stars are rapidly rotating near main-sequence Be stars of luminosity classes III–V that are characterized by strong hydrogen Balmer emission lines, which are often variable on a wide range of timescales (see Underhill & Doazan 1982 for a review). Be stars possess large excess IR emission (compared with their photospheric emission), which is interpreted as arising from free-free emission in an extended circumstellar envelope (Wright & Barlow 1975). Other observational evidence pointing to the existence of an extended circumstellar structure includes the aforementioned Hα emission-line profiles, as well as UV wind lines (Snow 1981). Be stars also show intrinsic (often variable) polarization with levels of up to 2%, and this polarization indicates that the envelope must be flattened (e.g., Coyne 1976). There is now direct evidence from interferometric Hα imaging that shows these envelopes are indeed quite flattened and are consistent with some kind of equatorial disk (Quirrenbach et al. 1994, 1997).

Determining the actual geometry of Be star disks has been the focus of many theoretical and observational investigations. In recent years, a dynamical model of the Be circumstellar environment has been developed that predicts the formation of a dense, geometrically thin equatorial disk—the wind-compressed disk (WCD) model (Bjorkman & Cassinelli 1993). In this model, the disk is formed by equatorial compression of a rapidly rotating, radiatively driven stellar wind. The analytic model presented by Bjorkman & Cassinelli predicted the formation of an equatorial disk with a half-opening angle of $\Delta\theta \approx 0°.5$. The wind compression mechanism was verified by numerical hydrodynamics simulations of rotating stellar winds (Owocki, Cranmer, & Blondin 1994), which confirmed the basic geometry and velocity structure, but found larger opening angles for the disk ($\Delta\theta \approx 3°$). Keplerian disks also predict small opening angles, but if these disks are isothermal, they flare at large radii (Hanuschik 1996). This flaring may help explain the low-velocity, deep absorption lines that are abundant in the so-called Be shell stars.

Recently, Owocki, Gayley, & Cranmer (1996) investigated the effect of nonradial forces on the efficiency of the wind compression mechanism when applied to radiatively driven winds. They found that these forces, which were not included in the original WCD investigations, may inhibit the formation of a wind-compressed disk. These results are dependent on the specific form of the line-driving mechanism and also on the optical depth of the wind. Based on these preliminary investigations, it is not clear whether or not the WCD model is applicable to Be stars if their winds are radiatively driven. However, alternate wind-driving mechanisms (e.g., pulsation) would not be subject to the specific nonradial forces considered by Owocki et al., possibly enabling wind compression to occur. Since we are investigating the general circumstellar geometry and not any particular model, our findings are observationally driven, and we note that the means of formation of Be circumstellar disks and whether they are Keplerian or wind-compressed disks is still unclear.

On the observational side, Waters (1986) derived the radial dependence of the circumstellar density from analysis of the slopes of the free-free continuum emission. In this analysis, he assumed that the circumstellar environment could be modeled by a wedge of opening angle 15° with a power-law parameterization for the radial density distribution. Although the slope of the free-free continuum determines the radial distribution of material, it provides no information about the disk opening angle (Schmid-Burgk 1982), so Waters' choice of 15° was somewhat arbitrary but motivated by the fraction of Be stars that show shell absorption features. More recently, Hanuschik (1996) has

[1] Present address: Ritter Observatory, Department of Physics and Astronomy, University of Toledo, Toledo, OH 43606-3390.

proposed opening angles of around 13° from shell star statistics. On the other hand, Doazan & Thomas (1982) proposed that the envelopes are only mildly flattened ellipsoids. The interferometric results (Quirrenbach et al. 1994, 1997) show that the opening angle of ζ Tauri's circumstellar envelope is less than 20°, but since these images are only resolved along one axis, the actual opening angle is unknown.

Early on, it was realized that polarization data, which samples material away from the direct line of sight to the star, could be a powerful diagnostic tool in the modeling of Be stars. Several spectropolarimetric modeling investigations have been conducted, with the most notable being that of Poeckert & Marlborough (1978), who constructed a circumstellar disk model to explain the continuum and line (Hα and Hβ) spectropolarimetric variations in γ Cas.

Since scattering-induced polarization samples material outside the direct line of sight, polarimetry provides a potentially very powerful diagnostic tool for determining the geometry of nonspherical circumstellar envelopes. However, polarization measurements alone cannot be used to constrain circumstellar geometries, since different geometries can produce the same level of polarization, and since the polarization is also sensitive to the viewing (inclination) angle of the system (see Brown & McLean 1977 for example). It is therefore essential to obtain additional information on the polarized system from other methods (e.g., spectroscopy) when seeking a unique solution.

Bjorkman & Cassinelli (1990) and Bjorkman (1992) investigated the relation between optical polarization (at 4050 Å) and 12 μm IR excess emission for disk-like circumstellar envelopes. Using a single-scattering analytic model of the polarization, combined with an analytic model of the optically thick IR emission, they found that the polarization and IR excess could be matched either by a disk of small opening angle and large optical depth or by a wide disk of small optical depth. The duplicity of the solutions arises because of polarimetric cancellation properties. For geometrically thin disks, the polarization (calculated in the single-scattering limit) is proportional to the electron number density (i.e., disk mass). As the opening angle is increased (for a fixed density), the polarization level rises because more electrons can contribute to the scattered polarization. As the opening angle becomes very large, polarization cancellation begins to occur between the positively polarized photons (polarized parallel to the rotational symmetry axis of the star) that are scattered in the equatorial regions of the disk and the negatively polarized photons (polarized perpendicular to the rotational symmetry axis) that are scattered into the observer's line of sight from higher latitudes in the disk. Thus, the polarization attains a maximum level, as a function of opening angle, and then decreases as the opening angle of the disk becomes very large, so that the envelope becomes spherically symmetric. Bjorkman & Cassinelli (1990) found that the opening angles of models required to match the observations were less than 15° for the thin disk and about 50° for the thick disk.

Bjorkman & Cassinelli (1990) used a single-scattering model, which overestimates the polarization level, and did not include the effects of attenuation within the envelope. In a later study, Waters & Marlborough (1992) also investigated the relation between optical polarization and IR excess emission. Their polarization calculations used the Poeckert & Marlborough code, which also assumes the single-scattering approximation; however, it includes an optical depth correction factor, $e^{-\tau}$, to account for radiation that is either scattered out of the observer's direction or absorbed by sources of continuous hydrogen opacity within the envelope. They found that with this "single-scattering plus attenuation" approximation, it was difficult to obtain high levels of polarization (above 1.5%), and they stated that any multiple scattering would only serve to reduce the polarization. For this reason, Waters & Marlborough were unable to place tight constraints on the disk geometry and could not rule out the possibility of circumstellar disks with opening angles in the range 10°–40°.

Our investigations into the polarization arising from multiple scattering in circumstellar envelopes (Wood et al. 1996a) have shown, however, that multiple scattering within the envelope actually serves to *increase* the polarization above the levels predicted by "single-scattering plus attenuation" approximations—in some instances doubling the polarization. This is due to the multiple scattering being biased to occur in a single plane (i.e., the disk). Multiple Thomson scattering within a single plane reduces the component of the electric vector parallel to the plane and leaves the perpendicular component unaltered—thus yielding a larger net polarization level than that from a single-scattering event. We therefore concluded that multiple scattering would allow some disk geometries to easily exceed the polarization levels observed in Be stars, thereby excluding a range of disk opening angles. We also investigated the polarized spectrum from envelopes that contained continuous hydrogen absorptive opacity and disk emission, which modifies the emergent polarized spectrum (Wood et al. 1996b). We found that, in addition to raising the overall polarization level, the combined effects of multiple scattering plus wavelength-dependent absorption yield larger (almost double) polarization jumps across the Balmer edge and give a steeper slope to the polarized continuum than that obtained from single-scattering calculations. An additional concern with the investigations by Bjorkman & Cassinelli and Waters & Marlborough is that the polarization and IR data are not simultaneous. Since Be stars are quite variable, there is no guarantee that the disk will have the same geometry at two different epochs.

With the wide spectropolarimetric wavelength coverage obtained from the University of Wisconsin's Pine Bluff Observatory (PBO), coupled with the effects of multiple scattering, we have found that the disk geometry can be constrained much more tightly than before, since we now have many more additional spectropolarimetric features to constrain the model: the polarization Balmer and Paschen jumps, and the slope of the polarized Paschen continuum—all determined by electron scattering modified by hydrogen continuous absorption and emission, as well as the IR excess determined by the free-free disk emission.

In this paper, we present a general scheme for quantitatively constraining the disk opening angle by using continuum spectropolarimetric data. We find that by matching polarization levels on either side of the Balmer jump, we again find two possible solutions for the disk opening angle (assuming the system inclination can be estimated). It is by matching the polarization data across the series limits that we can reduce the number of possible solutions.

To demonstrate our modeling technique for a specific case, we use new and archival spectropolarimetric data to model the circumstellar geometry of the Be star ζ Tau. We find that the optical data (from 3200 Å to 1.05 μm) can be reproduced with either a geometrically thin ($\Delta\theta = 2^\circ.5$) or a geometrically thick ($\Delta\theta = 52^\circ$) circumstellar disklike geometry. However, these two solutions differ in the IR. The thin disk solution is found to match the *IRAS* fluxes, while the thick disk produces a factor of 2 too much emission; thus, the IR discrepancy favors the thin disk solution. In addition, the recent results on optical interferometric imaging of Be stars (Quirrenbach et al. 1994, 1997) have shown that the circumstellar envelope of ζ Tau is flattened with a half-opening angle of less than 20° (assuming an inclination that is close to edge-on), which is consistent with our thin disk solution and well below our thick disk solution. Combining our new modeling technique with the interferometry indicates conclusively that the Be circumstellar environment must be geometrically thin and necessarily rules out any geometrically thick ellipsoidal shell models.

2. SPECTROPOLARIMETRIC MODELING

The general picture of the Be circumstellar environment is that of a two-component wind model (see Waters & Marlborough 1994 for a review) comprising a fast, optically thin polar region (where the UV wind lines are formed) and a slower, denser equatorial disk (where the polarization and IR excess emission arises). Keeping within the framework of this general picture, we assume that the circumstellar density can be parameterized by

$$\rho = \rho_0\left(\frac{R_*}{r}\right)^n (1 + A \sin^m \theta) . \qquad (1)$$

This parameterization yields a dense equatorial disklike structure superimposed on a spherically symmetric region, and allows for geometrically thin (large m) or geometrically thick (small m) disks with small or large equator-to-pole density ratios, depending on the adopted A-value. When investigating a particular star, the radial density exponent, n, may be derived from the slope of the free-free continuum as in Waters (1986), with values typically in the range $2 < n < 3.5$. In our investigations, we fix the equatorial-to-polar density ratio at 1000 ($A = 999$), which is the value inferred from comparisons of the UV and IR mass-loss rates (Lamers & Waters 1987). Note that with this large a density contrast, essentially no scattering occurs in the polar regions; similarly, little IR emission is produced in the polar regions, so our model is insensitive to the value of A, when A is large.

The wavelength dependence of the continuous hydrogen opacity at optical wavelengths is included, as in Bjorkman & Bjorkman (1994) and Wood et al. (1996b), according to

$$\rho\kappa_\nu = a_{\text{f-f}}\left[1 - \exp\left(-\frac{h\nu}{kT}\right)\right]\frac{n_e^2}{\nu^3 T^{1/2}} + \begin{cases} n_2 a_2\left(\frac{\nu_2}{\nu}\right)^3 + n_3 a_3\left(\frac{\nu_3}{\nu}\right)^3 + n_4 a_4\left(\frac{\nu_4}{\nu}\right)^3 , & (\nu > \nu_2) , \\ n_3 a_3\left(\frac{\nu_3}{\nu}\right)^3 + n_4 a_4\left(\frac{\nu_4}{\nu}\right)^3 , & (\nu_2 > \nu > \nu_3) , \\ n_4 a_4\left(\frac{\nu_4}{\nu}\right)^3 , & (\nu_2 > \nu > \nu_4) , \end{cases} \qquad (2)$$

where the first term is due to free-free and the second is due to bound-free absorption. The free-free absorption coefficient is $a_{f\text{-}f} = 3.692 \times 10^8$ cm^5 s^{-3} k$^{1/2}$, and the photoionization cross sections are $a_2 = 1.4 \times 10^{-17}$ cm^2, $a_3 = 2.2 \times 10^{-17}$ cm^{-2}, and $a_4 = 3.2 \times 10^{-17}$ cm^2 at the Balmer, Paschen, and Brackett thresholds, respectively.

The hydrogen level populations, n_i, are determined from a simple scaling law that is fitted to the detailed non-LTE populations calculated using a spherically symmetric non-LTE ionization code (MacFarlane 1992) for the equatorial density (eq. [1] evaluated at $\theta = 90°$). The scaling law was that chosen by Cassinelli, Nordsieck, & Murison (1987), who observed that although the hydrogen lines are quite optically thick, the non-LTE populations are approximately determined by a simple balance between photoionizations and recombinations. Thus, we approximate the level populations using

$$n_i = \frac{q_i n_e^2}{W} \; (i = 2, 3, 4) , \qquad (3)$$

where $W = 0.5\{1 - [1 - (R_*/r)^2]^{1/2}\}$ is the dilution factor. The scaling coefficient, q_i, was chosen so that the approximation formula (3) reproduces the same radial optical depth as the spherically symmetric non-LTE calculation. In other words, q is obtained from the relation

$$\tau_{\text{b-f}} \propto \int_{R_*}^{1.7R_*} n_i \, dr = q_i \int_{R_*}^{1.7R_*} \frac{n_e^2}{W} \, dr , \qquad (4)$$

where the hydrogen level populations, n_i, are those from the spherically symmetric code. The upper limit on the radius ($1.7R_*$) is set to the location where most of the polarization is produced (Cassinelli et al. 1987). Note that with this choice of q, the approximation formula (3) reproduces the spherically symmetric non-LTE populations within a factor of about 2 over the range $1.1R_* < r < 5R_*$. The q-values depend on the stellar spectral energy distribution, as well as the temperature and density of the circumstellar envelope, and were recalculated for each run in our model-fitting procedure (see Table 1).

In the UV and optical, the opacity is given by equation (2), but for IR wavelengths, the bound-free opacity takes a form similar to the free-free opacity, such that the total

TABLE 1

THERMAL EMISSION COEFFICIENTS FOR THE CIRCUMSTELLAR DISK

γ (Å)	γ_ν (10^{-40} ergs cm^3 s^{-1} Hz^{-1}) $T_* = 20{,}000$ K	$T_* = 19{,}000$ K
1500	0.427	0.365
2000	1.910	1.806
2600	5.546	5.460
3122	9.610	10.120
3640	14.477	16.669
3650	2.011	1.937
4000	2.494	2.438
4500	3.200	3.182
5696	4.870	4.970
7000	6.534	6.813
8200	7.884	8.326
8215	3.983	4.028
9000	4.381	4.458
10000......	4.840	4.959

hydrogen absorptive opacity is given by

$$\rho\kappa_\nu = a_{\text{f-f}}(g_{\text{f-f}} + g_{\text{b-f}})\left[1 - \exp\left(-\frac{h\nu}{kT}\right)\right]\frac{n_e^2}{\nu^3 T^{1/2}} \quad (\nu < \nu_4)\,, \tag{5}$$

where $g_{\text{f-f}}$ and $g_{\text{b-f}}$ are free-free and bound-free Gaunt factors, respectively (see Table 2). Diffuse envelope emission, which balances the bound-free and free-free absorption, is included according to the emissivity formula from Osterbrock (1989):

$$j_\nu = \frac{1}{4\pi}\,\gamma_\nu(H^0,\, T)n_e^2\,, \tag{6}$$

where $\gamma_\nu(H^0, T)$ is presented in his Table 4.7 or may be calculated using his equations (4.21) and (4.22). The values we used for our model fitting are shown in Table 3.

Having set up the circumstellar geometry and opacity, we then proceed with the Monte Carlo radiation transfer as outlined in Wood et al. (1996a, 1996b). The number of envelope photons to be released, relative to the number of stellar photons, is obtained by taking the ratio of envelope luminosity to stellar luminosity at each wavelength. We assume that the circumstellar envelope is isothermal and that its luminosity is determined by integrating equation (6) over the volume of the envelope for the given wavelength and temperature under investigation. For the stellar luminosity, we use the relevant Kurucz model atmospheres for the spectral type and luminosity class of the underlying star (Kurucz 1994). The Monte Carlo simulation then provides us with the emergent F/F_* at discrete wavelengths (see Fig. 6 below); multiplying our output by the stellar spectrum, we obtain the emergent spectrum, corrected for the effects of scattering, *continuous* absorption, and *continuous* reemission by the circumstellar envelope. Since our simulation uses fewer frequency points than the model atmosphere, we interpolate our calculated F/F_* values to the wavelength points of the Kurucz stellar atmosphere models, and then multiply to obtain our emergent flux spectra. Note that this procedure does not include line emission or Doppler shifts associated with the envelope rotation and expansion.

TABLE 2

FREE-FREE PLUS BOUND-FREE GAUNT FACTORS[a]

γ (μm)	$g_{\text{f-f}} + g_{\text{b-f}}$
12	2.38
25	2.44
60	2.61

[a] From Allen 1973

TABLE 3

COEFFICIENTS q_i (cm^3) FOR NON-LTE HYDROGEN LEVEL APPROXIMATION

	T_* (K)	
COEFFICIENT	20,000	19,000
q_1	1.69×10^{-18}	2.64×10^{-18}
q_2	6.51×10^{-21}	4.67×10^{-21}
q_3	2.63×10^{-21}	1.79×10^{-21}
q_4	1.75×10^{-21}	1.66×10^{-21}

With these assumptions, we then proceed to fit the polarization Balmer jump by varying the opening angle of the disk and the equatorial electron scattering optical depth (i.e., varying m and ρ_0 in eq. [1]). As we described above, due to polarimetric cancellation properties, polarimetric data at a given wavelength can be reproduced with many different circumstellar geometries and optical depths. However, the presence of continuous hydrogen opacity and the resulting polarization jumps that occur across series limits enable us to constrain the geometry to only two disk opening angles (assuming an inclination angle and a circumstellar structure given by eq. [1]). This is demonstrated in Figures 1 and 2, where we have plotted the ratio of the polarization on either side of the Balmer jump (Fig. 1) and the polarization level just longward of the Balmer jump (Fig. 2) for various optical depths and disk half-opening angles. In each of these figures, we have assumed that the inclination is 82° and that the equator-to-pole density ratio is 1000. The spectral type, disk temperature, and the various opacity coefficients are those that we derived for the thin disk solution for ζ Tau (see § 4 and Tables 1, 2, and 3). Note that we have held the q-values constant for all optical depths and opening angles in these figures. In reality, the q-values are a weakly varying function of circumstellar density, and in our model fits in § 4, we do recalculate them for each density investigated.

In Figure 1, we see that, as the equatorial electron scattering optical depth is increased, the polarization Balmer jump ratio is also increased. This occurs because the increased optical depth yields a higher hydrogen absorptive opacity shortward of the jump, attenuating more of the scattered (polarized) photons and so resulting in a smaller polarization level. Longward of the jump, where the hydrogen opacity is small, increasing the electron optical depth results in more scattering, but without much attenuation of the scattered photons, and hence increases the polarization. The net result of both of these effects is to increase the polarization ratio with increasing optical depth. This effect can be seen in Figure 1 for all opening angles. Note that, for very large opening angles, the polarization ratio becomes very large and may even flip negative when the equatorial regions become very optically thick shortward of the jump. This occurs for large optical depths because most of the scattered photons only reach the observer via scattering in the polar regions of the circumstellar envelope, producing negative polarization (i.e., perpendicular to the rotation axis). Such polarization reversals are not observed in Be stars (this implies an upper limit for the optical depth), so we only plot positive polarization ratios.

Clearly, for any observed polarization Balmer jump ratio, there exist many opening angles and optical depths that can reproduce the polarization ratio. However, in Figure 2 we demonstrate that *for a given polarization ratio*, there exist only two opening angles that can reproduce the polarization level longward of the Balmer jump. This figure plots the polarization at 3650 Å as a function of disk opening angle for various values of the polarization Balmer jump ratio, R_{BJ}. Note that, for a given polarization level, there are only two solutions for the opening angle; this is the duplicity of solutions that exist because of the polarimetric cancellation properties discussed previously. These curves have a similar form to those presented by Waters & Marlborough

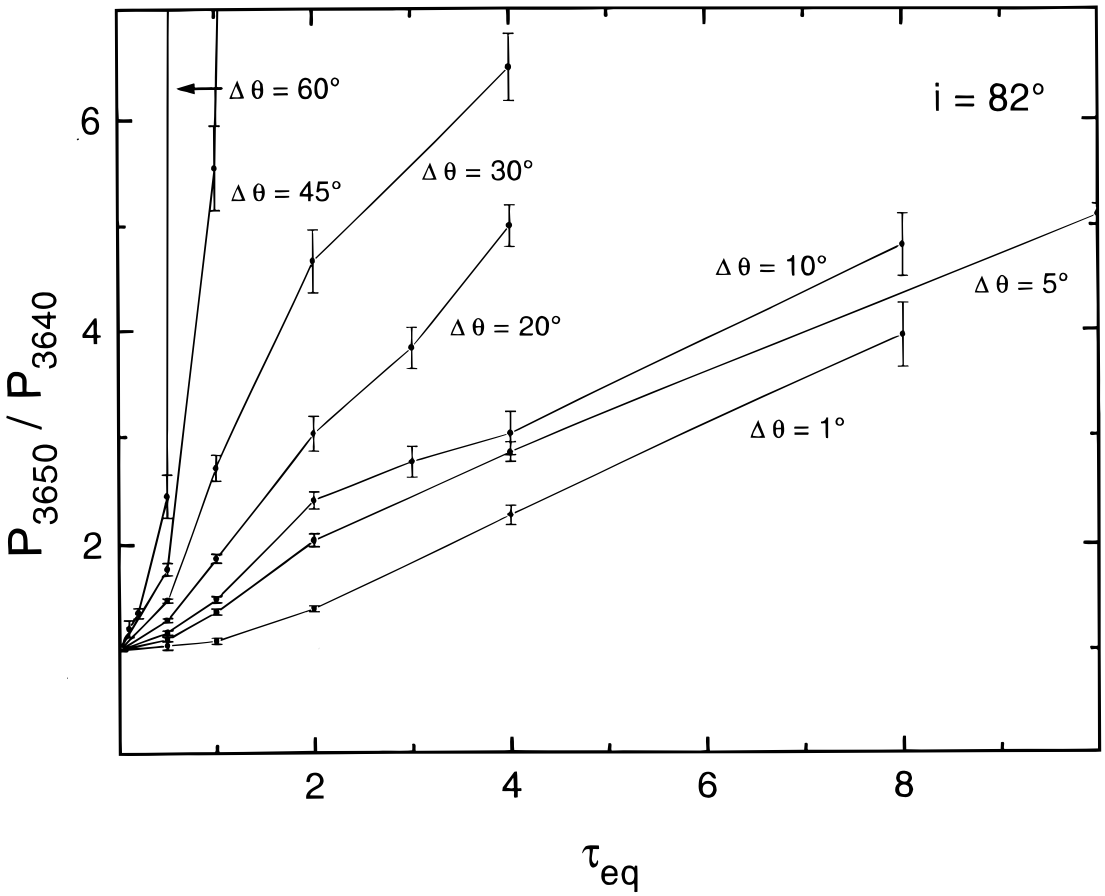

FIG. 1.—Polarization Balmer jump ratio, P_{3650}/P_{3640}, vs. equatorial electron scattering optical depth, τ_{eq}, for different disk opening angles, $\Delta\theta$

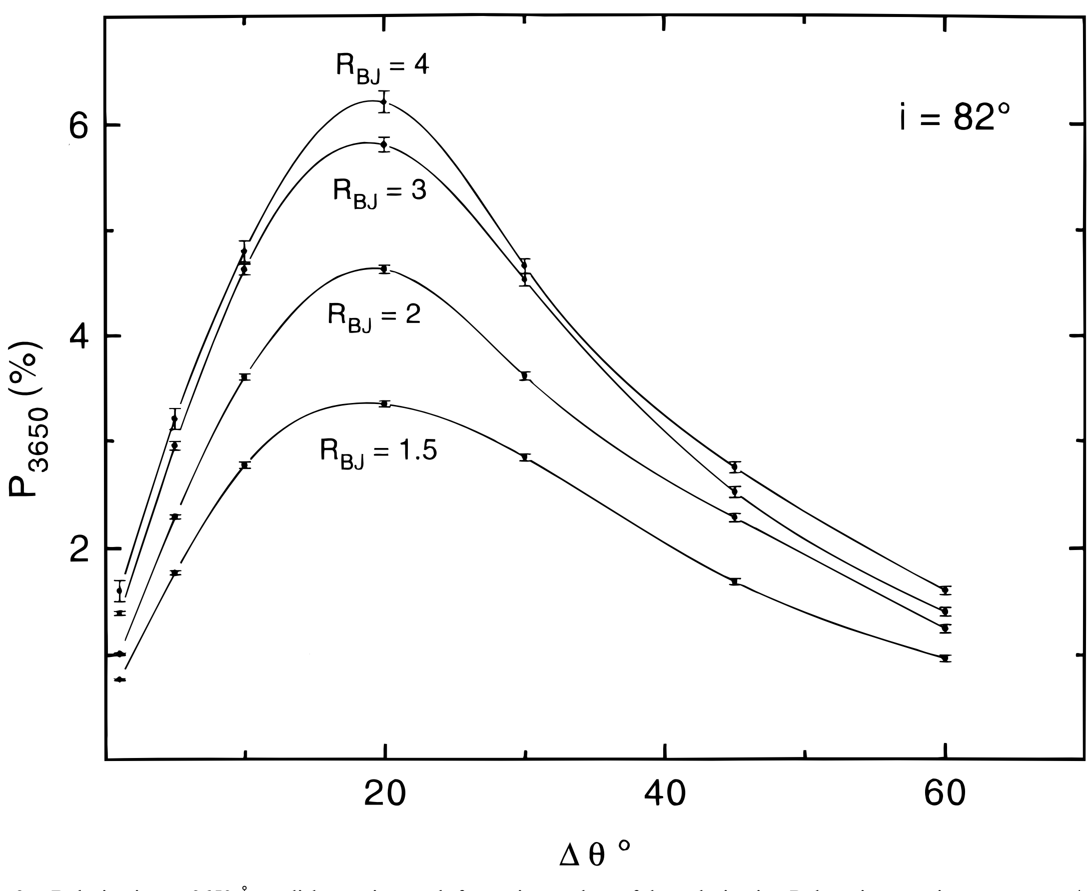

FIG. 2.—Polarization at 3650 Å vs. disk opening angle for various values of the polarization Balmer jump ratio, $R_{BJ} = P_{3650}/P_{3640}$

(1992; their Fig. 1), but note that the multiple scattering can yield very large polarization values (in excess of 6%) compared with their maximum of about 2% from the single-scattering plus attenuation calculations. Note that since the polarization levels observed in Be stars are at most 2%, Figure 2 enables us to immediately discount circumstellar envelopes with opening angles in the range 10°–40°, since these produce too much polarization. The result of these two figures is that, provided we have a reasonable estimate of the disk inclination, we may determine the disk opening angle and optical depth from analysis of the polarization Balmer jump.

Once we have matched the polarization Balmer jump, we then attempt to match the flux Balmer jump. We choose to fit the flux Balmer jump rather than the slope of the optical continuum since the size of the jump is insensitive to the somewhat uncertain interstellar reddening. Similarly, the size of the polarization Balmer jump is insensitive to the interstellar polarization. Having obtained matches to both the polarization and the flux Balmer jumps, we then calculate the spectrum covering the entire PBO wavelength range. In order to calculate the flux and polarization spectra, we must adopt temperatures for the star and disk, and these temperatures will change the size of both the flux and the polarization Balmer jumps (as well as the slope of the continuum spectral energy distribution). Thus, by matching the flux Balmer jump, we may constrain the stellar spectral type. Normally, one would not attempt to determine the spectral type of a Be star by the size of its Balmer jump (or the slope of its spectral energy distribution, i.e., $B-V$) because of the uncertainty of the envelope effect, but since we are explicitly including the envelope emission and absorption, we are accounting for the intrinsic reddening and filling-in of the Balmer jump. Note that we must simultaneously fit both the polarization and the observed flux spectrum; therefore, we must iterate the stellar temperature and disk density and opening angle until we obtain a consistent solution. In the following sections, we apply the above modeling scheme to the optical spectropolarimetric data of ζ Tau.

3. ζ TAU: STELLAR PARAMETERS

The star ζ Tau (HD 37202) was classified by Slettebak (1982) as a B1 IVe-sh star with a $v \sin i$ of 220 kms s^{-1}. However, there is a great deal of ambiguity regarding its spectral classification, with different investigations yielding spectral types in the range B1–B4 with luminosity classes from II to V (Herbig & Spalding 1955; Stock 1956; Mendoza 1956; Blaauw 1956; Bonsack & Stock 1957; Lesh 1968). More recently, Slettebak (1994) proposed a UV classification scheme that utilized the ratios of UV line equivalent widths. Based on this scheme and using Slettebak's (1994) measurements for the equivalent widths for ζ Tau, we obtained the line ratios for ζ Tau presented in Table 4. The spectral type for each ratio was obtained from the correlations shown in Slettebak's (1994) Figure 3. Taking a weighted average, we derive a spectral type for ζ Tau of B2.9 ± 0.4. We also adopt a luminosity class IV (the most frequently quoted value), for which the stellar radius is $R_* = 5.5\ R_\odot$ (Straizys & Kuriliene 1981).

TABLE 4

RATIO OF EWS AND DERIVED SPECTRAL TYPES FOR ζ TAU

Atomic Lines (Å)	EW Ratio[a]	Spectral Type[b]
Si II λ1265/Si III λ1299	0.84	2.5 ± 0.5
C II λ1334/C III λ1175........	0.72	2.4 ± 0.5
Al II λ1671/Al III λ1863	0.71	4.0 ± 0.5
Fe II λ2599/Fe III λ1601......	0.55	2.6 ± 1.0

[a] From Slettebak 1994.
[b] Based on the UV classification scheme of Slettebak 1994.

The largest source of error in our modeling scheme arises from the uncertainties in the luminosity class and hence the stellar radius. We find that the derived disk densities and opening angles are very sensitive to the stellar radius, as is now explained. The polarization level is governed essentially by the electron optical depth (e.g., Brown & McLean 1977) that scales with the stellar radius; that is, $P \propto n_e \sigma_T R_*$. Similarly, the polarization Balmer jump is sensitive to the hydrogen optical depth, $\tau_{\text{b-f}} \propto \rho \kappa_\nu R_* \propto n_e^2 R_*$ (see eqs. [2] and [3]). Substituting $n_e \propto P/R_*$ then yields a $1/R_*$ dependence to the hydrogen optical depth. Thus, increasing the stellar radius increases the polarization and decreases the Balmer jump. To compensate for this, we must increase the optical depth (to restore the Balmer jump), but this raises the polarization even further, so we must at the same time reduce the disk opening angle to prevent the polarization from being too large. Therefore, to match the polarization level and polarized Balmer jumps of stars with larger radii, we require denser, thinner disks (Putman et al. 1996). For this reason, we feel that the uncertainty in stellar radius arising from the poorly determined luminosity class is the largest source of systematic error in our modeling procedure.

Finally, we assume that the circumstellar geometry can be parameterized by equation (1) and set the equator-to-pole density ratio to be 1000. The radial exponent of the density parameterization is taken to be $n = 3$ following Waters (1986), who derived this value for ζ Tau from analysis of the slope of its IR continuum.

3.1. ζ *Tau: Observations*

The star ζ Tau has been studied polarimetrically by many authors, first with optical broadband polarimetry (e.g., Capps, Coyne, & Dyck 1973) and later with optical and UV spectropolarimetry (Bjorkman et al. 1991). The optical polarization spectrum clearly exhibits the characteristic shape caused by Thomson scattering modified by continuous hydrogen absorptive opacity. For the purposes of the present study, we have used new, moderate-resolution optical spectropolarimetry of ζ Tau using the half-wave plate spectropolarimeter (HPOL) on the 0.9 m telescope of the University of Wisconsin's PBO, combined with new data from the Wisconsin Ultraviolet Photopolarimeter Experiment (WUPPE), obtained during the Astro-2 space shuttle mission.

In its new configuration (Nordsieck & Harris 1996), HPOL provides polarimetric spectral coverage from about 3200 Å out to 1.05 μm. A thick CCD detector is used with two separate gratings to provide this coverage in two pieces, one covering 3200–6200 Å and the other covering 6000–10500 Å. The observations were made through a 6″ × 12″ aperture, providing polarimetric spectral resolution (based on 3 pixels per resolution element) of about 9 Å in the blue and 12 Å in the red. For details on the instrument design and capabilities, see Nordsieck & Harris (1996). The data were reduced using standard calibration and reduction techniques developed specifically for HPOL (see Wolff, Nordsieck, & Nook 1996).

The optical data presented here is a combination of two PBO observations from 1995, bracketing the time of the Astro-2 mission. The first observation was made on 1995 March 3, and the second was made on 1995 March 18. The polarimetric differences between the two observations were small (less than 0.1% change in the overall level of polarization), so we have combined them to improve the signal-to-noise ratio and to average out any small variability around the time of the UV observation.

The UV data shown here were obtained by WUPPE on Astro-2 on 1995 March 8. WUPPE provides spectropolarimetric data from about 1450 to about 3200 Å, with a resolution of about 16 Å. The data were calibrated using a combination of pre- and post-flight laboratory measurements, plus in-flight observations of flux standards and polarization standard stars. Instrumental effects, including instrumental polarization, have been removed in the data reduction process. For further details on the instrument, see Nordsieck et al. (1994).

Figure 3 presents the UV and optical spectropolarimetric data on ζ Tau obtained from WUPPE and PBO, prior to any removal of interstellar contamination. The top panel shows the flux, and the bottom panel shows the polarization in percent, all as a function of wavelength. Note the presence of large discontinuities at the Balmer and Paschen edges in the polarization spectrum—this is characteristic of electron scattering modified by continuous hydrogen absorptive opacity. In the UV, the polarization spectrum is dominated by the effects of metal line blanketing, as first noted by Bjorkman et al. (1991), which causes the depressions observed in the polarization spectrum around 1700 and 1900 Å.

In addition to the optical and UV data, we have included archival infrared observations at 12, 25, and 60 μm, taken from the *IRAS* Point Source Catalog (Beichman et al. 1988). The inclusion of the *IRAS* data provides a very broad wavelength range over which to fit the models, which in turn provides better constraints to the determination of acceptable models.

3.2. ζ *Tau*: *Dereddening and Removal of Interstellar Polarization*

Since Be stars have extended circumstellar environments, any reddening will consist of both an intrinsic component (due to the circumstellar envelope) and an interstellar component. Therefore, we cannot attribute the measured $E(B-V)$ to interstellar dust entirely when dereddening flux observations. To independently estimate the relative contributions of intrinsic and interstellar reddening, we apply the correlation, $N_{\rm H\,I} = 4.8 \times 10^{21}$ cm^{-2} $E(B-V)$, between H I column density, $N_{\rm H\,I}$, and $E(B-V)$, derived by Bohlin, Savage, & Drake (1978). They measured the interstellar H I column density towards ζ Tau to be $N_{\rm H\,I} = 1.1 \times 10^{20}$ cm^{-2}, which gives an estimated $E(B-V) = 0.02$ for the interstellar reddening contribution.

In addition to reddening, the interstellar medium (ISM) also polarizes light passing through it. This contamination due to interstellar polarization is removed using the scheme

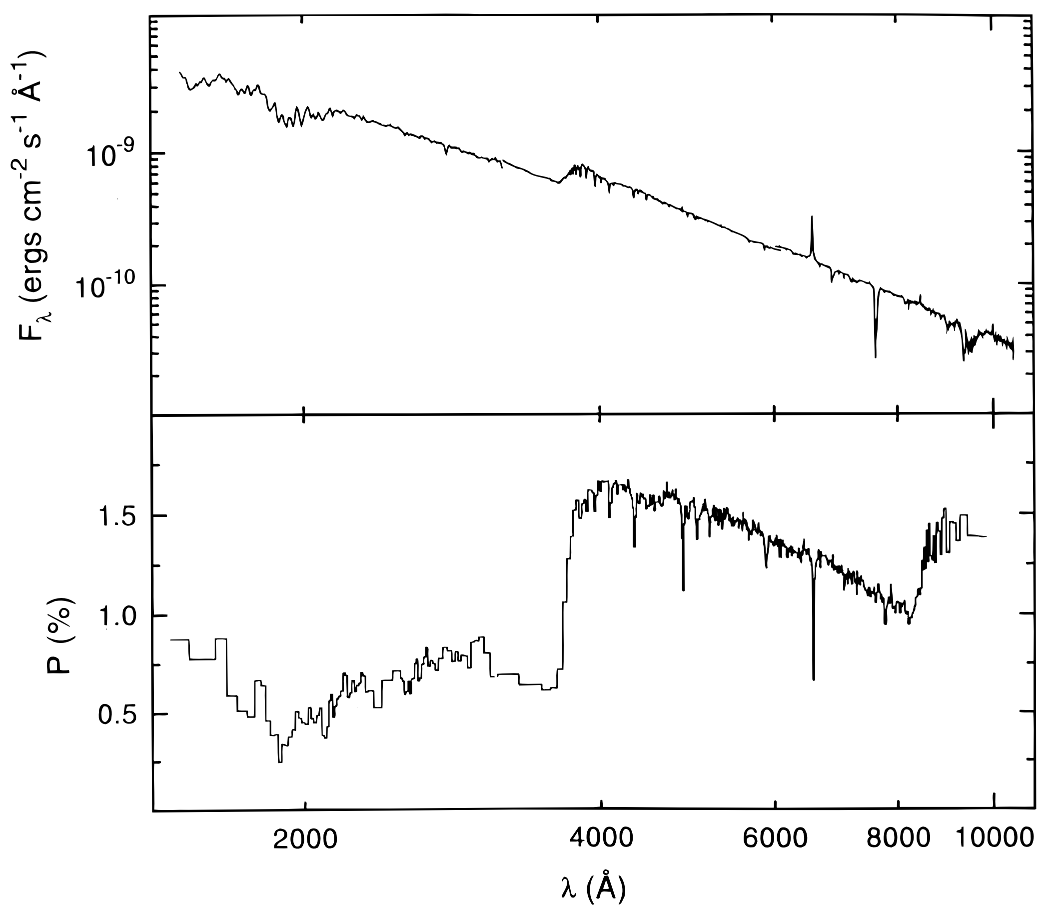

FIG. 3.—WUPPE and PBO spectropolarimetry of ζ Tau before correction for interstellar reddening and interstellar polarization. The top panel shows the flux, and the bottom shows the percent polarization.

outlined in Quirrenbach et al. (1997). The polarization change across the Balmer jump enables the determination of the intrinsic polarization position angle, which is found to be $\psi_* = 32°$ for ζ Tau. The component of the ISM polarization perpendicular to the intrinsic direction has its maximum value $P^{\perp}_{\max} = 0.04\%$, at a wavelength $\lambda_{\max} = 7100$ Å. The interstellar position angle, from measurements of field stars, is $\psi_{\rm ISM} = 11° \pm 5°$, which implies that the parallel component of the interstellar polarization is $P^{\parallel}_{\max} = 0.04\%$, yielding a total interstellar $P_{\max} = 0.06\% \pm 0.02\%$. The value obtained for $P_{\max}$ allows us to perform a consistency check on the $E(B-V)$ value, since interstellar polarization is at most 9% per $E(B-V)$ (Serkowski, Mathewson, & Ford 1974), implying that $P_{\max} < 0.2$. Our estimate is about one-third of this maximum value—perhaps a bit lower than average, but certainly not unreasonable. We then estimate the ratio of selective-to-total extinction from the relation $R_V = 5.5\ \mu{\rm m}^{-1}\ \lambda_{\max}$ (Serkowski et al. 1974), and find that $R_V = 3.9$ for ζ Tau's sight line. Having obtained $E(B-V)$, R_V, $\lambda_{\max}$, $P_{\max}$, and $\psi_{\rm ISM}$, we then deredden the observations using the Cardelli, Clayton, & Mathis (1989) formulae and remove the interstellar polarization using the Wilking et al. (1980) modification to the Serkowski et al. (1974) law for the interstellar polarization.

4. OPTICAL CONTINUUM SPECTROPOLARIMETRY AND *IRAS* FLUX MODELING OF ζ TAU

Throughout the data-modeling process, we assume that the circumstellar envelope is isothermal with a temperature of $0.8T_*$ (Klein & Castor 1978). The stellar temperature is determined by iteration, using our scheme described in § 2, until we obtain a good match for the continuum flux Balmer jump and polarization Balmer jump. This involves recalculating the values of q in equation (3) and γ in equation (5) for each stellar temperature and disk density that we investigate. We have also assumed that ζ Tau is observed close to edge-on. This is a reasonable assumption, since ζ Tau is a shell star and also because it lies near the top of Cote & Waters' "triangle diagram" (Cote & Waters 1987), which plots the correlation between polarization and IR excess; stars near the top are thought to be edge-on, while stars near the bottom are pole-on; this is supported by the results from the optical interferometry (Quirrenbach et al. 1997). Proceeding with the scheme outlined above, we found the two solutions (geometrically thick and thin equatorial circumstellar disks) that reproduced the polarization Balmer jump in ζ Tau. We then computed the continuum polarization and flux over the entire WUPPE plus PBO wavelength range, as well as the *IRAS* wavelengths for each of these geometries. The results are shown in Figures 4 and 5 and summarized in Table 5. We found that the best fit to the continuum flux spectrum of ζ Tau was obtained for stellar temperatures of 19,000 and 20,000 K for the geometrically thin and thick disk solutions, respectively.

TABLE 5

SUMMARY OF MODEL FITS[a]

Model	m	$\Delta\theta$ (deg)	$\tau_{\rm eq}$ (electron)
Thin disk	700	2.5	3.0
Thick disk	1.4	52	0.5

[a] For the circumstellar geometry of ζ Tau for an inclination $i = 82°$, equator-to-pole density ratio of 1000, and $1/r^3$ radial dependence for the density.

In Figure 6, we show our calculated F/F_* values as a function of wavelength for both the thin and the thick disk solutions. Note that the thick disk increases the size of the flux Balmer jump, while the thin disk solution decreases slightly the size of the Balmer jump. Therefore, compared with the thin disk solution, the thick disk solution requires an earlier spectral type (reducing the photospheric Balmer jump) for the underlying star in order to match the observed size of the Balmer jump. Also note that at long wavelengths, the slope of the thick disk solution is steeper than that of the thin disk, yielding a small discrepancy in the near-IR that grows to a factor of 2 disparity between the two solutions at *IRAS* wavelengths.

Since the Kurucz model atmospheres modified by the circumstellar disk provide the emergent flux, we must multiply our calculated fluxes by $(R_*/D)^2 = 4\theta_*^2$ to match the observations, where θ_* is the angular diameter. We find that the angular diameter required to match the model and data is $\theta_* = 0.48 \pm 0.06$ mas. This value is a bit larger than previous estimates of 0.4 mas (Wesselink, Paranya, & De Vorkin 1972) and 0.43 mas (Underhill et al. 1979), but it agrees within the errors. The reason for our slightly larger angular diameter is that our model has accounted for the effects of disk absorption and emission that are nonisotropic. Using our assumed stellar radius of $R_* = 5.5\ R_\odot$, we find an Earth-star distance of $D = 110$ pc, which corresponds to a parallax of 9 mas. This is remarkably close to the 8 mas listed in Lang (1991), but other observations of the parallax yield values ranging from 3 ± 5 mas (van Altena, Truen-liang Lee, & Hoffleit 1991, as cited in Kuin et al. 1995) to 13 mas (Rimmer 1930). In principle, these parallax and angular diameter measurements can be used to determine the radius and hence luminosity class of ζ Tau. Of course, the large errors on the parallax measurements render it almost impossible to constrain the stellar radius accurately. Improved observational data, such as that which will come from *Hipparcos* and new interferometry, may help constrain the models further.

In Figure 4*a*, we see that the simulated thin disk spectrum (*thick line*) matches the optical data (*thin line*) and *IRAS* data very closely, with the size of the Balmer jump and the slope of the Paschen and *IRAS* continua agreeing with the observations. (In our model-fitting scheme, we match the polarization and flux Balmer jumps; therefore, the Paschen slope, Paschen jump, and *IRAS* fluxes provide an independent check for our model.) On closer inspection, we find that the hydrogen absorption lines are deeper in the model than in the data (Hα is in emission in the data, and in absorption in the model), but this can be interpreted as filling-in of the photospheric absorption lines by disk line emission. Also note that the observed polarization Balmer jump is rounded, whereas the model jump is sharp. Again, this is due to the absence of line effects in our model; the confluence of the Balmer lines yields a rounding-off of the polarization Balmer jump. Similarly, the wavelength of the observed flux Balmer jump is shorter than that of the model atmosphere. Since the observed wavelength of the Balmer jump can be used as a measure of the surface gravity (pressure broadening or density) of a stellar atmosphere (Barbier & Chalonge 1939, 1941; see also Stromgren 1963, pp. 151–154), this difference indicates that the disk density is lower than that of the stellar atmosphere—quantitative

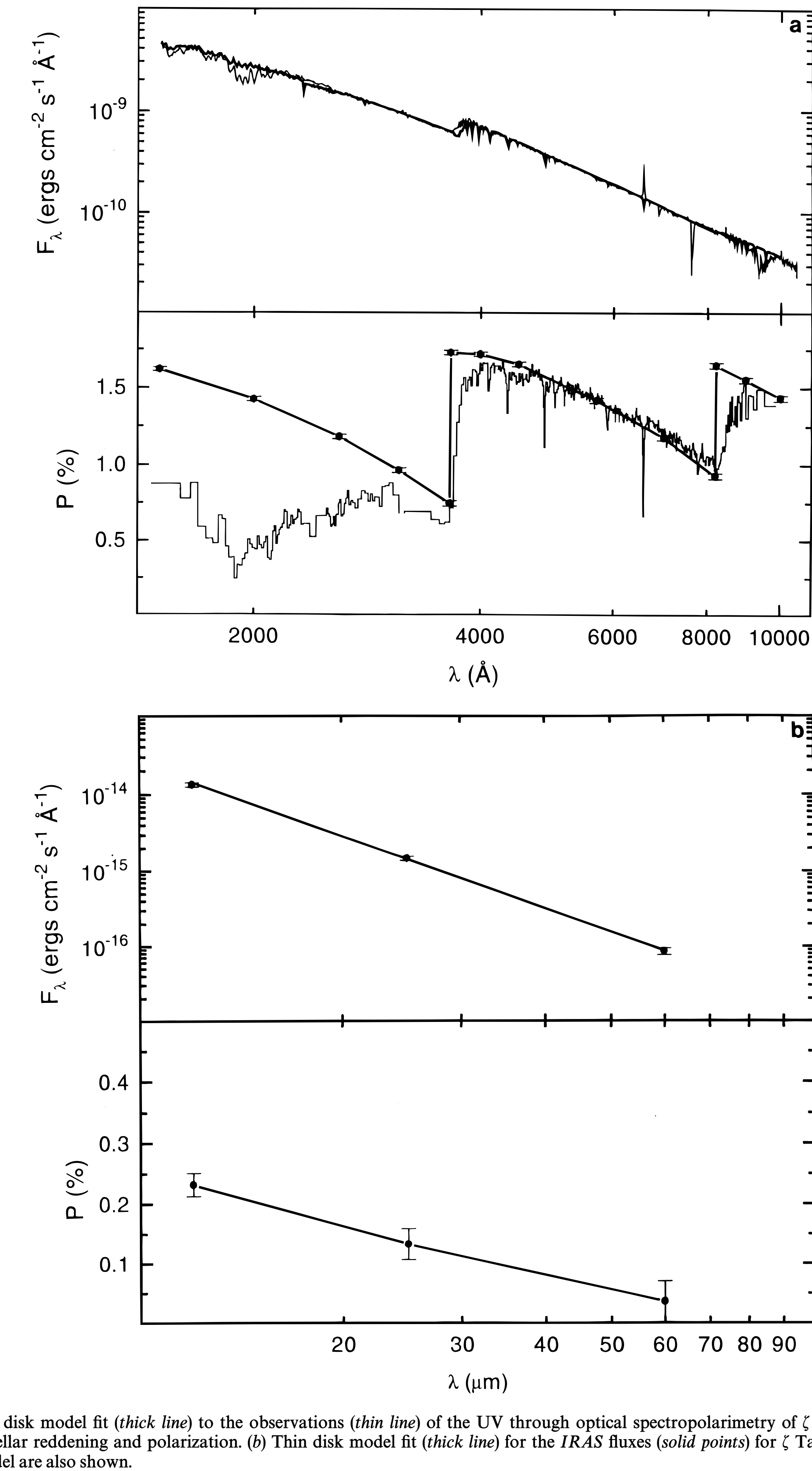

FIG. 4.—(*a*) Thin disk model fit (*thick line*) to the observations (*thin line*) of the UV through optical spectropolarimetry of ζ Tau. The data have been corrected for interstellar reddening and polarization. (*b*) Thin disk model fit (*thick line*) for the *IRAS* fluxes (*solid points*) for ζ Tau. The polarization levels predicted by the model are also shown.

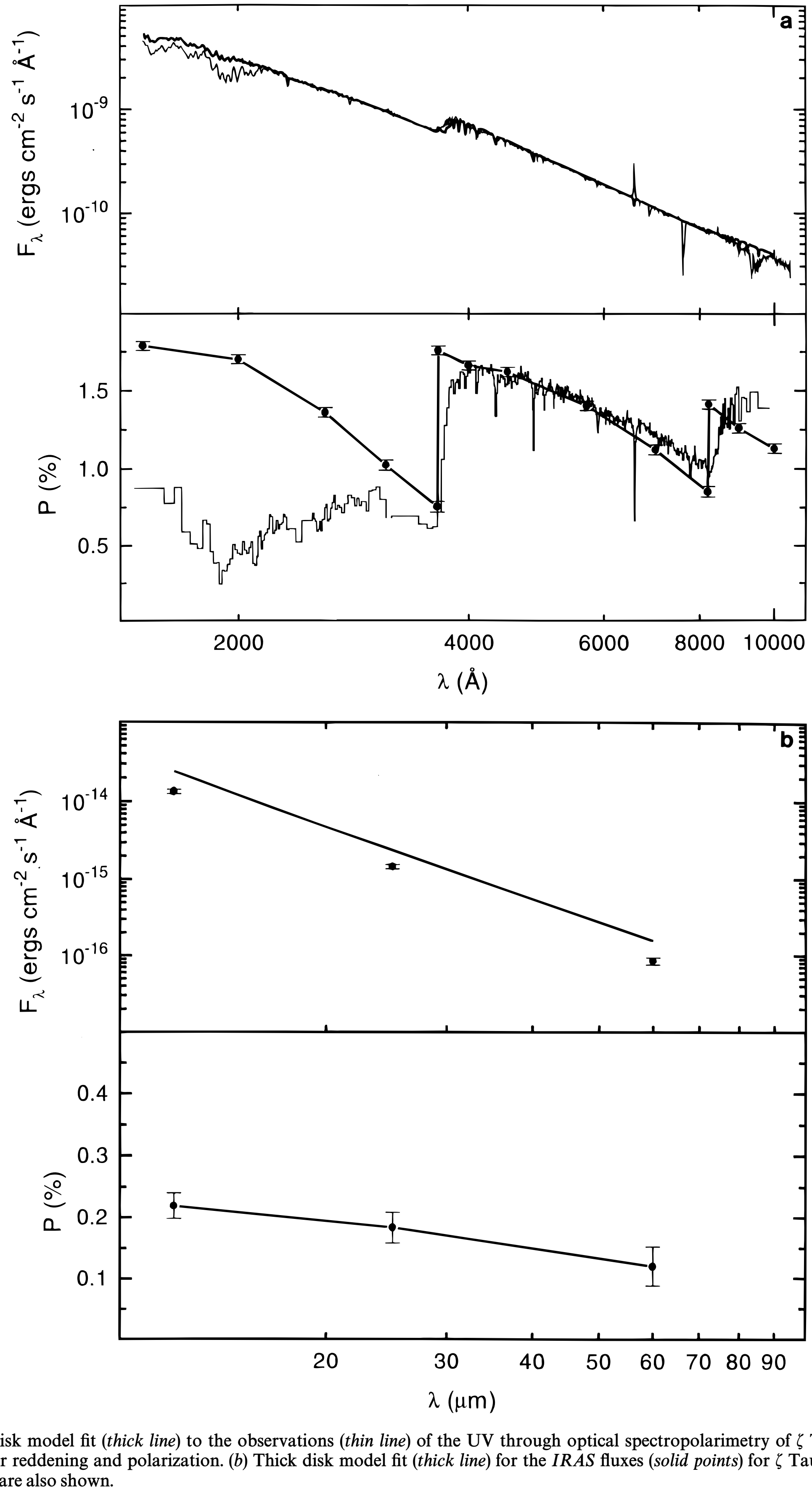

FIG. 5.—(*a*) Thick disk model fit (*thick line*) to the observations (*thin line*) of the UV through optical spectropolarimetry of ζ Tau. The data have been corrected for interstellar reddening and polarization. (*b*) Thick disk model fit (*thick line*) for the *IRAS* fluxes (*solid points*) for ζ Tau. The polarization levels predicted by the model are also shown.

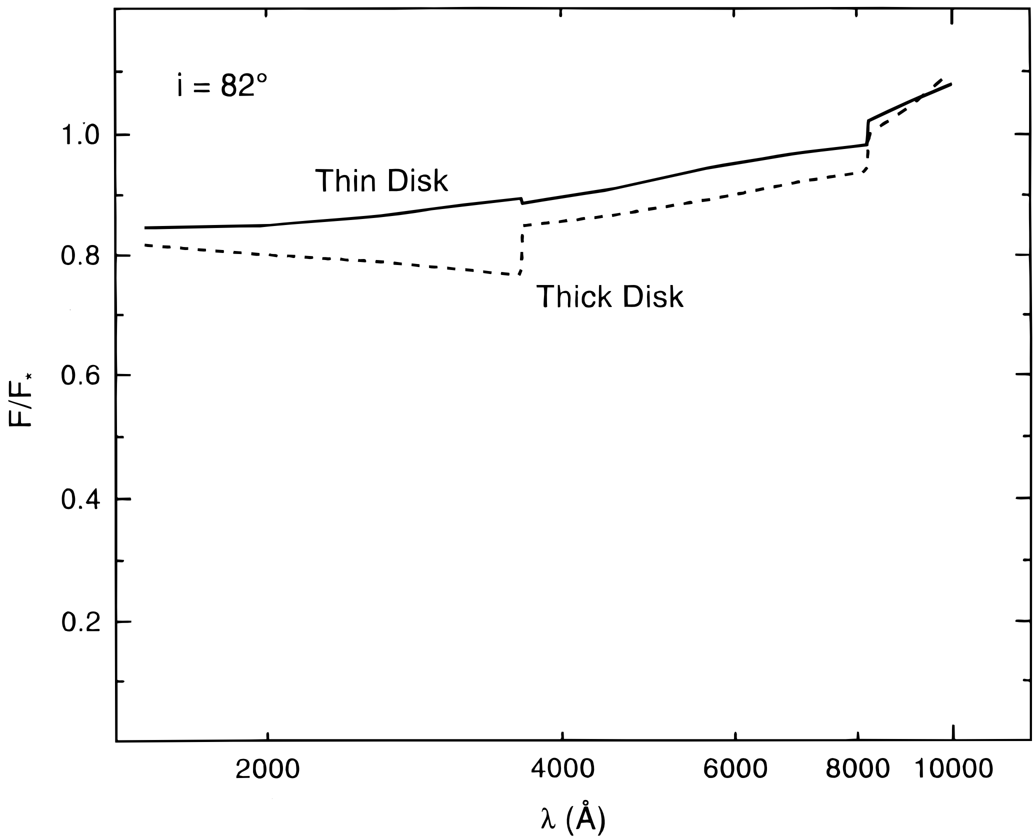

FIG. 6.—Effect of circumstellar envelope on the emergent stellar flux for the thin and thick disk solutions

modeling of this effect may provide additional information on the density within the disk. However, since we have included only *continuum* absorption and emission from the disk, we are not attempting to fit the line profiles (that effort is underway but is beyond the scope of the present paper), and these discrepancies between the model and the observed line profiles are to be expected. In particular, the model shows large departures from the data in the UV at the wavelengths where the metal line complexes are strongest.

The thin disk solution for the optical spectropolarimetry (Fig. 4*a*) has an opening angle of 2°.5 ($m = 700$) and an equatorial electron scattering optical depth of $\tau_{eq} = 3$, while the thick disk solution (Fig. 5*a*) has an opening angle of 52° ($m = 1.4$) and an equatorial electron scattering optical depth of $\tau_{eq} = 0.5$, both for an inclination of $i = 82°$. Based on these optical spectropolarimetric modeling results alone, we cannot distinguish between a thick or a thin circumstellar geometry. At this point, we must appeal to other observations.

The strongest observational evidence that will enable us to discriminate between the thick and the thin disk solutions is the recent optical interferometric images of Be stars (Quirrenbach et al. 1994, 1997). Images of ζ Tau in the light of Hα emission show it is elongated, with its short axis aligned with the intrinsic polarization position angle—indicating a disklike geometry. Since the image is unresolved along its short axis, only an upper limit of $\Delta\theta < 20°$ can be placed on the half-opening angle of the disk. This limit is much smaller than our thick disk solution, which indicates that the thin disk solution is the appropriate one for ζ Tau.

Additional supporting evidence for the thin disk solution is obtained from the flux data. Although the thick disk flux spectrum shows a good match to the Balmer jump and UV continuum, we find that, on close inspection in the near-IR, the thick disk model is starting to diverge from the data and produces too much emission. This is especially evident at the *IRAS* wavelengths (Fig. 5*b*) where the thick disk model produces a factor of 2 too much flux—the thick disk has a large volume, so it produces too much free-free *IRAS* flux. If the temperature of the thick disk were reduced to around 9000 K, then the model *IRAS* emission might be able to match the data. However, preliminary investigations into the UV line–blanketed polarization (Bjorkman & Wood 1996) indicate that such a cool disk would not be able to reproduce the UV metal line–blanketed depolarizations that are present in ζ Tau, and that higher disk temperatures are required to match the UV data (see below). On the other hand, the thin disk solution matches both the near-IR and the *IRAS* data (Fig. 4*b*) very well. (As a caveat, however, we must note that the *IRAS* data are not contemporaneous with the spectropolarimetry.) Combining the disk temperature constraint for the UV depolarization with the results of optical interferometry and *IRAS* flux modeling, we infer that the thin disk is the more likely solution.

We have also calculated the polarization at *IRAS* wavelengths (Figs. 4*b* and 5*b* and find that the polarization levels are a few tenths of a percent at these wavelengths. This result is in contrast to previous calculations that predicted zero polarization at long wavelengths (e.g., Waters & Marlborough 1992). At *IRAS* wavelengths, the emission from the circumstellar envelope dominates the stellar flux, and previous models assumed that this envelope emission would escape without scattering and therefore yield zero polarization. In contrast, our models show that this IR emission is scattered and yields significant (potentially measurable) IR polarization levels.

On the other end of the spectrum, our results also estimate the UV continuum spectropolarimetry (shown in Figs. 4*a* and 5*a*) from the same electron scattering plus hydrogen opacity model used to calculate the optical and IR spectra. Clearly, this model is inadequate for the UV wavelength regime where additional depolarizing effects are important. Bjorkman & Bjorkman (1994) investigated the role that gravity darkening may play on the UV depolarization but concluded that this was unlikely to be the dominant depolarizing effect. In the UV region observed by WUPPE, there are many metal line blends that provide additional absorptive opacity, and this line blanketing is the crucial missing ingredient from our model. Our preliminary efforts at modeling the UV polarization while including the effects of metal line blanketing (Bjorkman & Wood 1996) indicate that, by matching the UV line depolarization, we may be able to determine the disk temperature. This is possible because the dominant ionization stages of the metal lines are sensitive to the disk temperature and density, with different line blends, and hence UV depolarization patterns, appearing at different wavelengths depending on the circumstellar temperature. These initial calculations indicate that the disk temperature must be greater than 10,000 K and less than about 20,000 K to reproduce the strong Fe III depolarization seen around 1900 Å in the spectrum of ζ Tau. Such a high circumstellar temperature would produce too much *IRAS* flux for the thick disk solution (which requires a cooler temperature of around 9000 K to match the observations), again favoring the thin disk solution. Finally, we anticipate that detailed modeling of the UV spectropolarimetry, including the metal line blanketing, will enable us to further constrain the disk temperature and density structure.

5. DISCUSSION

In the previous section, we conducted a spectropolarimetric investigation into the circumstellar geometry of ζ Tau, using a Monte Carlo radiation transfer code that calculates the emergent flux and polarization, including the effects of multiple scattering, absorption, and emission from within an extended circumstellar envelope (this code also includes the scattering of disk emission, which we have found to be especially important for calculating the IR polarization). By fitting the continuum polarimetry and the continuous spectral energy distribution over the entire wavelength range from the UV through far-IR, we have been able to constrain the circumstellar geometry quantitatively.

5.1. *Circumstellar Geometry*

We found that the polarization Balmer jump can be reproduced using either a geometrically thick (half-opening angle $\Delta\theta = 52^\circ$ with an equatorial Thomson scattering optical depth $\tau_{\rm eq} = 0.5$) or a geometrically thin ($\Delta\theta = 2\overset{\circ}{.}5$, $\tau_{\rm eq} = 3$) circumstellar disk. The duplicity of the solutions arises because of the polarimetric cancellation properties discussed in § 1. We were able to further constrain the disk geometry by modeling the IR excess emission, and we found that the thin disk produces free-free fluxes that agree well with the *IRAS* data, while the thick disk produces a factor of 2 too much emission at these wavelengths. Recent optical interferometry provides supporting confirmation that rules out the thick disk option provided by our optical spectropolarimetric modeling.

The implications of this model fitting are that either Keplerian or wind-compressed disks may exist around Be stars, whereas geometrically thick ellipsoidal shell models are necessarily excluded. The opening angles predicted by the WCD model are typically 3° (Owocki et al. 1994), while Keplerian disks also have opening angles close to the star of around 3°, but Keplerian disks flare at large radii. Such flaring could possibly explain the low-velocity, low ionization state shell absorption features present in some Be stars. However, since the scattered polarization is governed by the disk shape close to the star, any flaring of a Keplerian disk at large radii would not be detected in the polarized spectrum. Therefore, our modeling of the continuum polarization data does not distinguish between Keplerian and wind-compressed disks. We conclude that the overall geometry of the circumstellar environment (i.e., the disk opening angle) is consistent with either a Keplerian or a wind-compressed disk, and is inconsistent with moderately flattened ellipsoids.

5.2. *Consistency Checks*

As part of determining the circumstellar geometry, we require seven parameters to completely specify a model: ρ_0, A, n, and m, in the density law (eq. [1]); T_* and R_* to specify the stellar parameters; and $T_{\rm disk}$ to specify the disk emission and absorption. As we discussed, the model is insensitive to the value of A (when A is large, as indicated by the UV vs. IR mass-loss rates), n is determined by the slope of the IR excess emission, R_* is determined from the (somewhat uncertain) luminosity class, and $T_{\rm disk}$ is set equal to $0.8T_*$. The remaining three free parameters (ρ_0, m, and T_*) are determined by fitting the polarization levels on both sides of the Balmer jump, and the size of the flux Balmer jump. Finally, the flux level determines the angular diameter, θ_*. In addition to the model parameters, we also require the levels of interstellar reddening and polarization, in order to compare the observations with our emergent flux and intrinsic polarization calculations. Since many of these parameters are poorly determined, it is desirable to make as many consistency checks as possible when fitting the data.

5.2.1. *Spectral Type*

The simplest check that we can perform is to verify that our effective temperature, T_* (determined by the size of the flux Balmer jump), agrees with other spectral classification methods. We find that for the thin disk solution, a stellar temperature of 19,000 K best reproduces ζ Tau's spectropolarimetry, while a temperature of 20,000 K gives the best fit for the thick disk solution. These stellar temperatures correspond to a spectral type a bit earlier than B3, which agrees with that obtained independently using Slettebak's (1994) UV line ratio classification scheme.

5.2.2. *Polarization Continuum Slope*

In our model, we have made a number of simplifying assumptions. For example, we have assumed that the hydrogen level populations can be represented by a non-LTE approximation obtained from a spherically symmetric model. We fitted the polarization Balmer jump, and the model then predicts the polarization Paschen jump and slope of the polarized Paschen continuum. These latter two quantities depend primarily on the value of n_3, while the first depends on n_2. Since the model successfully reproduces all three of these polarimetric features, this provides evidence that our non-LTE approximations successfully reproduce the ratio of n_3 to n_2. Note, however, that if one carefully examines Figures 4*a* and 4*b*, the Paschen slope is a little too steep, indicating that n_2 is underpopulated relative to n_3. This could be a consequence of using a spherically symmetric non-LTE model. Using the correct geometry will redirect some of the photoionizing radiation away from the equator. Reducing the equatorial photoionization rates will increase all the level populations. However, these non-LTE effects have a stronger influence on the lower levels, so the ratio n_2/n_3 will be enhanced.

5.2.3. *IR Excess*

Another assumption that we made was that the disk was isothermal with $T_{\rm disk} = 0.8T_*$. Although this was motivated by theoretical considerations, the actual value is somewhat arbitrary. Since the thermal free-free emission depends on the disk temperature, fitting the *IRAS* flux level shows that our choice is appropriate for the thin disk solution. On the other hand, the thick disk solution does not agree with the *IRAS* data (Fig. 5*b*). We could lower the disk temperature until the model and data agree, but this would require a disk temperature below the lower limit indicated by the UV line depolarization features. Finally, we note that the model slope agrees with the data, which verifies our value for the radial density exponent, *n*.

5.2.4. *Reddening*

The excess IR emission arises from an extended circumstellar envelope. This envelope emission and absorption also contaminates the optical region of the stellar spectrum. This intrinsic reddening poses difficulties for estimating interstellar reddening as well as estimating spectral types from the stellar colors. Our modeling technique enables us to determine quantitatively the envelope contribution to the reddening. We find from Figure 6 that the disk contamination in ζ Tau yields an intrinsic $E(B-V) = -2.5 \log (F_B F_{*V}/F_{*B} F_V) = 0.04$, which, using $(B-V)_0 = -0.21$ (Fitzgerald 1970) for the spectral type of ζ Tau, implies that $(B-V)$ would be -0.17 in the absence of any interstellar reddening. Using Figure 3, we calculated synthetic photometry for ζ Tau (using the Bessel 1990 *B* and *V* passbands) and find that the observed $(B-V) = -0.16$, yielding an interstellar $E(B-V) = 0.01$, which is consistent with our estimate of $E(B-V) = 0.02$ from the interstellar $N_{\rm H\,I}$.

5.2.5. *Flux Continuum Slope*

The reddening changes the slope of the flux continuum, which also depends on several other factors. These include the stellar temperature, the disk absorption and reemission, the interstellar reddening, and the color calibration of the observations. The slope of our model flux predictions agrees with the observations, which implies that our dereddening, stellar spectral type, and disk temperature are all compatible.

5.2.6. *Angular Diameter*

Finally, our angular diameter agrees with previous estimates. This checks the absolute flux calibration and also provides a minimal check of the stellar radius. Using the angular diameter, $\theta_* = (0.48 \pm 0.06)$ mas, with our adopted stellar radius of $R_* = 5.5\, R_\odot$ yields a distance of $D = 110$ pc and a parallax of 9 mas, which is consistent with the previous measurements in the literature, but these values cannot constrain the stellar radius to better than a factor of about 3.

6. CONCLUSION

This paper has addressed the problem of quantitatively determining the circumstellar structure of Be stars. We have used a detailed optically thick, multiple scattering model to fit the observed continuum spectropolarimetry of ζ Tau. In reproducing its continuous spectral energy distribution from the UV through *IRAS* wavelengths, and combining this with recent interferometric imaging, we have shown that the circumstellar environment comprises a geometrically thin disk and that geometrically thick disks or ellipsoidal shells are not acceptable solutions. Furthermore, the quantitative estimate of the disk opening angle, $\Delta\theta = 2^\circ.5$, is consistent with either a Keplerian disk or a wind-compressed disk. We also suggest that refining this technique to include the effects of line blanketing will ultimately provide a means of constraining the physical parameters of the circumstellar envelope.

The Be star spectropolarimetric database now spans the range 1450 Å to 1.05 μm for over a dozen stars (Bjorkman et al. 1996), with optical spectropolarimetry (from PBO) existing for over 40 additional stars. Further spectropolarimetric modeling, as described in this paper, as well as extensions to include metal line blanketing in the UV are already underway and promise to provide a powerful diagnostic tool in determining both the density and the temperature structure of the Be circumstellar environment. Our preliminary estimates (Putman et al. 1996) indicate that at least three additional Be star disks have opening angles less than about 3°, and future modeling efforts will be required to determine whether this is a common feature of most Be star disks.

We would like to thank Barbara Whitney, Mary Putman, Art Code, Ken Nordsieck, Joe Cassinelli, and John Mathis for discussions relating to this paper. In addition, we are grateful to the PBO observing team and data analyzers, in particular, Marilyn Meade, Brian Babler, and Nicolle Zellner. This research was funded by a UK SERC postdoctoral research fellowship (K. W.), NSF grant AST 91-15375 (J. E. B.), NASA grant NAGW-2921 (K. S. B), and NASA contract NAS 5-26777 to the University of Wisconsin.

I, Kenneth Wood, am taking this opportunity to acknowledge the many long and varied discussions I had with my close friend Jason Cardelli over the last five years. Jason died suddenly on the 14 May 1996 at age forty. Although our research did not overlap, Jason realized the potential behind the Monte Carlo techniques that I have been developing and we had discussed the possible application of these methods in his own field of interstellar medium studies. Jason's sudden and untimely death has robbed many people of a very special friend and colleague. Personally I learned a lot from Jason and feel that my research has benefited from his enthusiasm and encouragement.

REFERENCES

Allen, C. W. 1973, Astrophysical Quantities (London: Athlone)
Barbier, D., & Chalonge, D. 1939, Ann. d'Astrophys., 2, 254
———. 1941, Ann. d'Astrophys., 4, 30
Beichman, C. A., et al. 1988, *IRAS* Point Source Catalog (RP-1190; Greenbelt: NASA)
Bessel, M. S. 1990, PASP, 102, 1181

Bjorkman, J. E. 1992, Ph.D. thesis, Univ. Wisconsin
Bjorkman, J. E., & Bjorkman, K. S. 1994, ApJ, 436, 818
Bjorkman, J. E., & Cassinelli, J. P. 1990, in Angular Momentum and Mass Loss from Hot Stars, ed. L. A. Wilson & R. Stalio, (Dordrecht: Kluwer), 185
———. 1993, ApJ, 409, 429
Bjorkman, J. E., & Wood, K. 1996, BAAS, 187, 1909
Bjorkman, K. S., et al. 1991, ApJ, 383, L67
———. 1996, in ASP Conf. Ser. 97, Polarimetry of the Interstellar Medium, ed. W. G. Roberge & D. C. B. Whittet (San Francisco: ASP), 197
Blaauw, A. 1956, ApJ, 123, 408
Bohlin, R. C., Savage, B. D., & Drake, J. F. 1978, ApJ, 224, 132
Bonsack, W. K., & Stock, J. 1957, ApJ, 126, 99
Brown, J. C., & McLean, I. S. 1977, A&A, 57, 141
Capps, R. W., Coyne, G. V., & Dyck, H. M. 1973, ApJ, 184, 173
Cardelli, J. A., Clayton, G. C., & Mathis, J. M. 1989, ApJ, 345, 245
Cassinelli, J. P., Nordsieck, K. H., & Murison, M. A. 1987, ApJ, 315, 290
Cote, J., & Waters, L. B. F. M. 1987, A&A, 197, 93
Coyne, G. V. 1976, in IAU Symp., 70, Be and Shell Stars, ed. A. Slettebak (Dordrecht: Reidel), 233
Doazan, V., & Thomas, R. N. 1982, in B Stars with and without Emission Lines, ed. A. Underhill (SP-456, Greenbelt: NASA)
Fitzgerald, M. P. 1970, A&A, 4, 234
Hanuschik, R. W. 1996, A&A, 308, 170
Herbig, G. H., & Spalding, J. F. 1955, ApJ, 121, 118
Klein, R. I., & Castor, J. I. 1978, ApJ, 230, 902
Kuin, N. P. M., et al. 1995, NASA Astronomical Data Center CD-ROM, Vol. 1
Kurucz, R. L. 1994, Solar Model Abundance Model Atmospheres, Smithsonian Astrophysical Observatory, CD-ROM No. 19
Lamers, H. J. G. L. M., & Waters, L. B. F. M. 1987, A&A, 182, 80
Lang, K. R. 1991, Astrophysical Data: Planets and Stars (New York: Springer)
Lesh, J. R. 1968, ApJS, 17, 371
MacFarlane, J. J. 1992, A&A, 264, 153
Mendoza, E. E. 1956, ApJ, 123, 54
Nordsieck, K. H., et al. 1994, Proc. SPIE, 2010, 2
Nordsieck, K. H., & Harris, W. 1996, in ASP Conf. Ser. 97, Polarimetry of the Interstellar Medium, ed. W. G. Roberge & D. C. B. Whittet (San Francisco: ASP), 100
Osterbrock, D. E. 1989, Astrophysics of Gaseous Nebulae and Active Galactic Nuclei (Mill Valley, CA: University Science Books)
Owocki, S. P., Cranmer, S. R., & Blondin, J. M. 1994, ApJ, 424, 887
Owocki, S. P., Gayley, K., & Cranmer, S. 1996, BAAS, 28, 881
Poeckert, R., & Marlborough, J. M. 1978, ApJ, 220, 940
Putman, M., et al. 1996, BAAS, 28, 913
Quirrenbach, A., Buscher, D. F., Mozurkewich, D., Hummel, C. A., & Armstrong, J. T. 1994, A&A, 283, L13
Quirrenbach, A., et al. 1997, ApJ, in press
Rimmer, W. B. 1930, Mem. Mt. Stromlo Obs., Vol. 1, Mem. 2
Schmid-Burgk, J. 1982, A&A, 108, 169
Serkowski, K., Mathewson, D. L., & Ford, V. L. 1974, ApJ, 196, 261
Slettebak, A. 1982, ApJS, 50, 55
———. 1994, ApJS, 94, 163
Snow, T. P. 1981, ApJ, 251, 139
Stock, J. 1956, ApJ, 123, 253
Straizys, V., & Kuriliene, G. 1981, Ap&SS, 80, 353
Stromgren, B. 1963, in Basic Astronomical Data, Vol. 3, ed. K. A. Strand (Chicago: University of Chicago Press), 123
Underhill, A. B., Divan, L., Prevot-Burnichon, M.-L., & Doazan, V. 1979, MNRAS, 189, 601
Underhill, A. B., & Doazan, V. 1982, in B Stars with and without Emission Lines (SP-456; Greenbelt: NASA)
Waters, L. B. F. M. 1986, A&A, 162, 121
Waters, L. B. F. M., & Marlborough, J. M. 1992, A&A, 256, 195
———. 1994, in IAU Symp. 162, Pulsation, Rotation, and Mass Loss in Early-Type Stars, ed. L. A. Balona, H. F. Henrichs, & J. M. Le Contel (Dordrecht: Kluwer), 399
Wesselink, A. J. Paranya, K., & De Vorkin, K. 1972, A&AS, 7, 257
Wilking, B. A., Lebofsky, M. J., Kemp, J. C., Martin, P. G., & Rieke, G. H. 1980, ApJ, 235, 905
Wolff, M. J., Nordsieck, K. H., & Nook, M. A. 1996, AJ, 111, 856
Wood, K., Bjorkman, J. E., Whitney, B. A., & Code, A. D. 1996a, ApJ, 461, 828
———. 1996b, ApJ, 461, 847
Wright, A. E., & Barlow, M. J. 1975, MNRAS, 170, 41